

## Video Article

# Whole Body and Regional Quantification of Active Human Brown Adipose Tissue Using $^{18}\text{F}$ -FDG PET/CT

Katherine Kim<sup>1</sup>, Shan Huang<sup>2</sup>, Laura A. Fletcher<sup>1</sup>, Alana E. O'Mara<sup>1</sup>, Ilan Tal<sup>3</sup>, Robert J. Brychta<sup>1</sup>, Aaron M. Cypess<sup>1</sup>, Kong Y. Chen<sup>1</sup>, Brooks P. Leitner<sup>1</sup>

<sup>1</sup>Diabetes, Endocrinology, and Obesity Branch, National Institute of Diabetes and Digestive and Kidney Diseases, National Institutes of Health

<sup>2</sup>National Cancer Institute, National Institutes of Health

<sup>3</sup>Division of Nuclear Medicine and Molecular Imaging, Department of Radiology, Beth Israel Deaconess Medical Center, Harvard Medical School

Correspondence to: Brooks P. Leitner at [Brooks.leitner@yale.edu](mailto:Brooks.leitner@yale.edu)

URL: <https://www.jove.com/video/58469>

DOI: [doi:10.3791/58469](https://doi.org/10.3791/58469)

Keywords: Medicine, Issue 146, Brown adipose tissue, cold-activation, adult human, fluorodeoxyglucose, positron emission tomography, computed tomography, obesity, thermoregulation

Date Published: 4/1/2019

Citation: Kim, K., Huang, S., Fletcher, L.A., O'Mara, A.E., Tal, I., Brychta, R.J., Cypess, A.M., Chen, K.Y., Leitner, B.P. Whole Body and Regional Quantification of Active Human Brown Adipose Tissue Using  $^{18}\text{F}$ -FDG PET/CT. *J. Vis. Exp.* (146), e58469, doi:10.3791/58469 (2019).

## Abstract

In endothermic animals, brown adipose tissue (BAT) is activated to produce heat for defending body temperature in response to cold. BAT's ability to expend energy has made it a potential target for novel therapies to ameliorate obesity and associated metabolic disorders in humans. Though this tissue has been well studied in small animals, BAT's thermogenic capacity in humans remains largely unknown due to the difficulties of measuring its volume, activity, and distribution. Identifying and quantifying active human BAT is commonly performed using  $^{18}\text{F}$ -Fluorodeoxyglucose ( $^{18}\text{F}$ -FDG) positron emission tomography and computed tomography (PET/CT) scans following cold-exposure or pharmacological activation. Here we describe a detailed image-analysis approach to quantify total-body human BAT from  $^{18}\text{F}$ -FDG PET/CT scans using an open-source software. We demonstrate the drawing of user-specified regions of interest to identify metabolically active adipose tissue while avoiding common non-BAT tissues, to measure BAT volume and activity, and to further characterize its anatomical distribution. Although this rigorous approach is time-consuming, we believe it will ultimately provide a foundation to develop future automated BAT quantification algorithms.

## Video Link

The video component of this article can be found at <https://www.jove.com/video/58469/>

## Introduction

The increasing prevalence of obesity worldwide<sup>1</sup> has prompted an investigation into novel therapeutics to prevent and ameliorate obesity and its associated complications. Obesity is due in part to excess energy stored in white adipose tissue (WAT) in the form of triglycerides<sup>2</sup>. Brown adipose tissue (BAT) differs from WAT most notably due to its higher mitochondrial content, smaller and multilocular lipid droplets, distinct anatomical distribution, greater sympathetic innervation, and heat generating ability. Although BAT was once thought to exist only in small mammals and newborn infants, the presence of functional BAT was confirmed in adult humans in 2009<sup>3,4,5</sup>. The thermogenic capacity of human BAT is not yet known, but extensive study in small animals has shown that non-shivering thermogenesis can constitute up to 60% of their metabolism during cold-exposure<sup>6</sup>. As a result, human BAT is now being explored as a target for the treatment and prevention of obesity and related disorders<sup>7</sup>. Several clinical studies have shown that BAT thermogenesis correlates with increased glucose uptake and energy expenditure upon activation by mild cold exposure<sup>8,9,10</sup>. Yet, BAT's contribution to cold-induced thermogenesis remains controversial<sup>11,12,13,14</sup>, with much debate centered around how to quantify human BAT<sup>15</sup>. To better understand if BAT thermogenesis can be harnessed to combat obesity, it is critical to have an accurate measurement of its volume and metabolic activity.

Obtaining precise measurements of BAT is challenging due to BAT's unique anatomical distribution in humans. BAT is distributed within the white adipose depots in the neck, thorax, and abdomen in sites that are inaccessible to uncomplicated biopsies<sup>14</sup>. Autopsies have been used to characterize BAT anatomically<sup>16</sup>, but are infeasible for most research laboratories doing large studies and cannot provide longitudinal or functional information. Since BAT has a similar density to WAT and can occur in narrow fascial layers or in small pockets interspersed with WAT<sup>16</sup>, it is difficult to identify using a single, conventional imaging technique. This heterogeneity also makes automatic quantification of BAT more difficult than quantification of homogenous structures such as the liver<sup>17</sup>.

To overcome these challenges, BAT volume and activity are commonly quantified by coupling computed tomography (CT) and positron emission tomography (PET). The radiolabeled glucose analog  $^{18}\text{F}$ -Fluorodeoxyglucose ( $^{18}\text{F}$ -FDG) is the most widely used tracer to study BAT metabolic activity<sup>18</sup>. Adipose tissue can be differentiated from other tissue and air based on density information provided by the CT image in Hounsfield units (HU). PET images show the amount of  $^{18}\text{F}$ -FDG taken up into a volume of tissue in units of standardized uptake values (SUV). Active BAT

can be separated from tissue with insignificant tracer uptake, including WAT and inactive BAT, by co-registering PET images with corresponding CT scans and choosing an appropriate SUV threshold.

Through this paper, we aim to provide a step-by-step approach with an instructional video that can be used by clinical researchers to quantify human BAT using  $^{18}\text{F}$ -FDG PET/CT scans. This image analysis technique is ideally used after subject(s) have been exposed to cold or treated with pharmacological BAT stimulants. Specifically, we demonstrate to users on how to construct regions of interest (ROIs) while minimizing false positives using a free, open-source image-processing software (ImageJ) with a specific plug-in ([petctviewer.org](http://petctviewer.org)). The result of this approach can be used to study BAT volume, activity (glucose uptake), and anatomical distribution in individual study subjects.

## Protocol

All PET/CT images shown in this manuscript were obtained from participants in National Institutes of Health protocol no. 12-DK-0097 (ClinicalTrials.gov identifier NCT01568671). All participants provided written informed consent, and all experiments were approved by the Institutional Review Board of the National Institute of Diabetes and Digestive and Kidney Diseases.

### 1. Software Installation

1. Download ImageJ from [imagej.net](http://imagej.net) or use the link in [petctviewer.org](http://petctviewer.org) to download Fiji.  
Note: The 64-bit version of ImageJ is required for sets with over 1000 images.
2. Download and apply the PET/CT Viewer Plug-in to ImageJ following the installation instructions on [petctviewer.org](http://petctviewer.org). Refer to this website for a comprehensive guide to PET/CT Viewer, and be sure to check for regular updates to the software and the link to general instructions (<http://sourceforge.net/p/bifijiplugins/wiki/Brown%20fat%20Volume/>).

### 2. Loading PET/CT Images

1. Upload the following three stacks of images into the PET/CT Viewer Plug-in: attenuation corrected PET (CPet), non-attenuation corrected PET (UPet), and attenuation corrected CT (CT). Upload images using one of two methods (**Figure 1**).
  1. Method 1: Drag-and-drop
    1. Drag-and-drop from file explorer CT, CPet, and UPet filesets.
    2. Click “yes” on the three prompts that appear (Open all X images in “folder” as a stack), leaving the checkboxes within the prompts unchecked.
    3. When all three image sets are loaded, go to the ImageJ toolbar, select “plug-ins”, and scroll down the drop-down menu to select “Pet-ct viewer”.
  2. Method 2: Read Studies from CD or location on disk:
    1. Assign a location name to the dataset in the “Setup” tab. Assign a “DICOM path” by clicking “Browse” and navigating to a high-level storage folder containing all image sets.  
Note: DICOM (Digital Imaging and Communications in Medicine) is a file format commonly used for medical images and the “DICOM path” refers to the set of folders that contains all raw DICOM images.
    2. Return to the “Read” tab where individual scans (from one subject and one date) will become selectable for image processing.
    3. Select the subject, press “Read,” and ImageJ will automatically upload all three associated sets and launch the PET/CT viewer.
2. Load a previously made set of ROIs back into the PET/CT viewer by clicking the “load” button on the “Brown fat, ROIs” editor.  
Note: ImageJ will only allow an ROI .csv file created from the current set of CT, CPET, and UPET images to be loaded.

### 3. Navigating the PET/CT Viewer Plug-in

1. Wait for the PET/CT viewer to appear after loading as a new window with three separate views of the PET/CT images, presented either individually or fused.
  1. Click the “MIP” button at the top left of the PET/CT viewer to replace one of the other two windows with a fused PET/CT view. However, if this button is only clicked once, the MIP will no longer be available.  
Note: The MIP or maximal intensity projection is a two-dimensional, full body image displaying only the pixels with highest intensity in each axial slice.
  2. Click the “MIP” button again to bring back the MIP; now views of the fused PET/CT, CT, and MIP should be available.
2. Switch the MIP image orientation with the “>>”, “F”, and “S” buttons at the top of the PET-CT viewer.
3. Change the orientation of the PET, CT, and fused PET/CT images to axial, coronal, or sagittal planes using the three buttons to the left of the magnifying glass.
4. Click on the magnifying glass on the toolbar at the top of the PET-CT viewer to switch the function of the mouse’s scroll wheel.
  1. Zoom in on all views (except the MIP) by scrolling with the magnifying glass selected.
  2. Navigate through slices on all views (except the MIP) by scrolling when the magnifying glass is not selected.  
Note: Clicking on the MIP will also change the PET and CT slices to the anatomical location at the level of the cursor.
5. Select “Edit” at the top left of the toolbar and select “Brown fat, ROIs” from the dropdown menu that appears. A new dialog box will appear. Make sure that the following options are selected before starting quantification:
  1. Check the “Use SUV” and “Use CT” checkboxes.
  2. Select one of the three voxel inclusion criteria (“Any”, “Average”, or “All”).

Note: "Any" was used in Leitner *et al.* 2017<sup>19</sup>. For a detailed explanation of other options, refer to petctviewer.org.

3. Select "Interior" to apply the BAT detection algorithm to examine the voxels inside (rather than outside) the area of the ROI.
6. Input SUV limits for BAT in the first row of free-text fields of this dialog box.
  1. Input an SUV lower limit normalized to the individual's measured or predicted lean body mass and an upper limit sufficient to accommodate high activity levels<sup>19,20</sup>.  
Note: BAT maximal SUVs as high as ~75 g/mL have been reported in previous studies<sup>17</sup>; thus, 100 g/mL is a reasonable upper limit.
7. Input the BAT density range in the second row of free-text fields.  
Note: A -300 HU lower limit and -10 HU upper limit were used in Leitner *et al.* 2017<sup>19</sup> and a range from -190 to -10 HU was also previously recommended<sup>21</sup>.
8. Check the checkbox located beneath "Vol\*mean" so that all voxels deemed to be BAT will be highlighted in blue while the "brown fat, ROI" window is open.  
Note: The SUVmax will appear in red and the adjustable number next to this checkbox dictates the thickness of the highlight.
9. Draw the ROIs
  1. Click the "Draw" button in the "brown fat, ROI" dialog box. All clicks made within the PET/CT viewer window will be considered points that make up ROIs.
    1. Click anywhere within one of the three views to begin drawing an ROI.  
Note: A minimum of three points is required to form an ROI. Double-click after the first or second point to automatically delete the points and leave ROI drawing mode.
    2. Close and store the ROI by double-clicking after defining more than two points.
10. Compiling ROIs to obtain total BAT volume
  1. Draw ROIs in the axial plane to obtain total BAT volume.  
Note: It is easiest to have a maximum of one ROI per axial slice. Including more than one ROI per slice may lead to inadvertent overlap. Voxels identified as BAT in overlapping regions would then be counted more than once toward total BAT volume.
  2. Set the starting and ending "slice limit" to the same slice, so that the ROI will only apply to the current axial slice (e.g. starting slice = 90 and ending slice = 90).
  3. Circle one depot of BAT (e.g. in the left supraclavicular region) without completing the ROI. Continue the ROI by extending a connecting line across the body to the distant segment of BAT. Enclose the second BAT depot and double click on the previously identified point at the start of the 2<sup>nd</sup> region. Adjust ROI points as necessary to further reduce the possibility of false positives.
  4. Label the ROI based on the anatomical level for future reference using the text box at the bottom left of the dialog box.
11. Deleting unwanted ROIs
  1. Remove an unwanted ROI right after completion.
    1. Double-click anywhere within the PET/CT viewer to complete the unwanted ROI.
    2. Click the button with the recycling bin icon in the "Brown fat, ROI" dialog box.
    3. Click "yes" when prompted whether or not the user wishes to remove the current ROI.
  2. Delete a previously-made ROI.
    1. Select the desired ROI using the up or down arrows next to the ROI number.
    2. Click the recycling button.  
Note: Once the ROI has been deleted, the numbers associated with each ROI greater than the deleted ROI will accordingly shift down in order (e.g. if ROI #2 is deleted, ROI #3 will become #2, and ROI #4 will become #3, and so on). Labeled ROIs make this process easier.
12. Saving ROIs
  1. Click the "Save" button and provide a file name to save completed ROIs in a .csv file.  
Note: It is recommended that ROIs be saved in intervals of 10 slices so that progress is not lost. The .csv files can be opened in a text editor or spreadsheet program and contains all relevant data about identified BAT in each ROI including volume, activity, SUVmean, etc. Changing values in a spreadsheet program may alter the file format and make it unreadable in ImageJ.

## 4. Quantifying whole-body BAT

1. Use these general guidelines to identify BAT in all regions of the body.
  1. Avoid sections of bordering tissue with high density or activity contrasts, as minute co-registration issues may introduce false positives.  
Note: Keep in mind that BAT depots are often symmetrical, a property that will aid in visual BAT identification.
2. Use unique anatomical landmarks such as vertebral shape, other bony structures, and the presence of organs to identify the current anatomical region. Avoid region-specific structures known to produce false-positives.
  1. Identify BAT in the cervical region (vertebrae C3-C7).
    1. Navigate to the axial view at the third cervical vertebra (C3).  
Note: C1-C2 regions may also contain BAT, but BAT detection is likely to be confounded by high uptake of FDG in brain and skeletal muscle.
    2. Begin the ROI on the lateral side of the adipose tissue depot, avoiding neck muscles around the spinous process of the vertebra, and creating a border just posterior to the lower edge of the mandible.
    3. Exclude the thyroid, which may have similar density and activity level as BAT (**Figure 2A and 2B**).

2. Identify BAT in the dorsocervical region (Vertebrae C5-C7).
  1. Include this small, subcutaneous depot of BAT.  
Note: It appears symmetrically within the subcutaneous fat of the back near C5-C7, **Figure 2B**.
  2. Carefully include subcutaneous adipose tissue only where metabolic activity occurs.
3. Identify BAT in the supraclavicular region (Vertebrae C7-T3; Anterior to Spine, Posterior to Mediastinum)
  1. Begin drawing the ROI one side most superficial, close to the highly active BAT region.  
Note: BAT may extend to the area around the head of the humerus.
  2. Avoid the area directly above the trachea, which contains the thyroid, and enclose the ROI so that false positives near the neck muscles and lungs are excluded.
4. Identify BAT in the axillary region (Vertebrae T3-T7).
  1. Find axillary BAT as a progression from the supraclavicular region.
  2. Select BAT near where the arm begins to separate from the torso, but avoid ribs and the lungs.  
Note: These fat depots will eventually transition to subcutaneous WAT on the midaxillary line.
5. Identify BAT in the mediastinal region (Vertebrae T1-T7; Anterior):  
Note: BAT may accumulate around the entirety of the sternum for some individuals.
  1. Select BAT where the sternum begins to appear at the beginning of T2 near the anterior-most region of the individual's thoracic cavity, and continue ROIs inferiorly until the end of the xiphoid process.
6. Identify BAT in the paraspinous region (Vertebrae T1-T12), by drawing ROIs around BAT surrounding the body, not the spinous process, of the vertebra.
  1. Begin including paraspinous BAT from the appearance of the first rib at the lower edge of C7.
  2. Do not include areas between ribs, where intercostal muscles are localized.
7. Identify BAT in the abdominal region (Inferior to T12).
  1. Avoid the ureters, which have a similar density to BAT and very high activity levels. (**Figure 2D**).
  2. Trace active fat directly surrounding the kidneys, until metabolic activity is no longer present.
  3. Adjust abdominal ROIs within this region to exclude the ureters if the SUVmax voxel appears within or near the medial portion of the kidneys.

## 5. Quality Assurance

1. Examine the MIP for any obvious false positives after ROIs have been drawn on all axial slices measured from the C3 vertebrae to around L3-4.
2. Ensure that the red SUVmax voxel is in a region that contains BAT, instead of structures such as the ureters, which display similar density values to BAT and very high SUV values.
3. Save the final .csv file when certain that all BAT has been identified and all false-positives have been excluded.

## 6. Segmenting BAT into Individual Depots

Note: The following section is focused only on quantifying regional depots of BAT<sup>17</sup>. The steps are not necessary to obtain whole body BAT volume and activity.

1. Generate a BAT mask in the "brown fat, ROI" editor (**Figure 1**).  
Note: The mask is defined as a regenerated PET image containing only SUV values for voxels confirmed as BAT within the ROIs created during the previous steps of this protocol. The SUV value for all other voxels is set to 0.
  1. Keep PET/CT Viewer open with all identified BAT or reopen PET/CT Viewer from the "Plug-Ins" drop down menu and load ROIs saved above.
    1. Open the three sets of the subject's scan.
    2. Open the "brown fat, ROI" dialog box.
  2. Select the "mask" tab and press "Make masked PET".
  3. Wait for an additional box to pop up, with the filename beginning with "DUP\_..."
  4. Close the PET/CT Viewer, but leave the individual boxes (with the CT and PET scans) open, and then re-open a new PET/CT Viewer window.
  5. Select the following three checkboxes in the dialog box that appears: the CT set, UPET set, and the latest CPET set (*i.e.*, the CPET set closest to the bottom of the list) - this is the file containing the mask generated earlier.
  6. Change the view of the PET/CT images to sagittal and start drawing all ROIs for region-wide analysis start at the same sagittal slice.  
Note: The MIP image orientation will not change. Also, the most central slice (*i.e.*, along the center of the spine) is a good starting location.
  7. Change slice limits to range from slice 1 to the last slice in the scan being analyzed.
  8. Uncheck the density (HU) threshold and change the lower limit of the PET (SUV) threshold to 0.01 SUV to exclude any non-BAT voxels, which now have an SUV value of 0. Check the box above the "Draw Next" button.

1. Label regions by typing the desired label (e.g. "cervical", "supraclavicular", etc.) into the text field at the bottom left of the "Brown fat, ROI" dialog box.
2. Draw and label the cervical ROI (**Figure 3a**) by beginning at the top of C3 and extending the ROI to C7, drawing a line under the body of C7 before closing the ROI.
3. Draw and label the supraclavicular ROI (**Figure 3b**).
  1. Begin at C7, but do not include the body of the thoracic vertebrae while extending the ROI to T3, then extend the left border of the ROI to the top of the manubrium of the sternum.
  2. Line the right border of the ROI up with the anterior edge of the body of the thoracic vertebrae included within this region.
4. Draw and label the axillary ROI (**Figure 3c**).
  1. Begin at T3, but do not include the body of thoracic vertebrae while extending the ROI to T7, then extend the left border of the ROI short of the body of the sternum.
  2. Line the right border of the ROI with the anterior edge of the body of the thoracic vertebrae included within this region.
5. Draw and label the mediastinal ROI (**Figure 3d**) by encompassing the entire sternum within a single ROI.
6. Draw and label the Paraspinal ROI (**Figure 3e**) beginning at T1, including all thoracic vertebrae (until T12) within the ROI.
  1. Line the left border of the ROI with the anterior edge of the body of the thoracic vertebrae. Extend the right border of the ROI so that all BAT in the region is included.
7. Draw and label the Abdominal ROI (**Figure 3f**) by beginning at the top of L1 and include any BAT that was not accounted for in any of the other previous regions within the abdominal ROI.
8. Draw and label the dorsocervical ROI (**Figure 3g**).
  1. Include the region of dorsal subcutaneous fat near the cervical and top of the paraspinal region; this is where the subject's body has made contact with the scanning bed.
9. Check "show all" to display the ROIs of all regions to line up all ROIs to prevent overlapping or under-estimation.
  1. Position the perimeter of adjacent ROIs flush with each other, so that no BAT is included in two regions, and that no BAT is missing from all regions.
  2. Observe the MIP from both the front and side views to check if all slices are being included in the delineated regions. Check the slice limits if there are areas that are not highlighted in blue (Step 6.2.2).
10. Save the final data into a new .csv file. This file will contain regional totals or averages for all BAT parameters from each identified depot.

## Representative Results

BAT is quantified through a series of post image-acquisition processing steps as shown in **Figure 1**. PET and CT thresholds are used to identify voxels that are metabolically active and have the density of adipose tissue. However, some voxels meeting these criteria can occur in anatomical locations not likely to contain BAT. To avoid these false positives, PET, CT, and anatomical information must all be considered when drawing ROIs (**Figure 2**). Several common regions to include and avoid when quantifying whole body BAT in cold-stimulated subjects are shown in **Figure 2**, such as metabolically active cervical BAT vs. salivary glands, vocal chords, and thyroid (**Figure 2A and 2B**); supraclavicular BAT vs. shivering muscle near borders of air and solid tissue (e.g. intercostal muscles) (**Figure 2C**); and abdominal BAT vs. the calyces of the kidneys as they clear labeled glucose (**Figure 2D**). After the ROI's of each axial slice are compiled, BAT depots can be segmented in the sagittal plane to examine intra-/inter-individual differences in regional BAT activation (**Figure 3**).

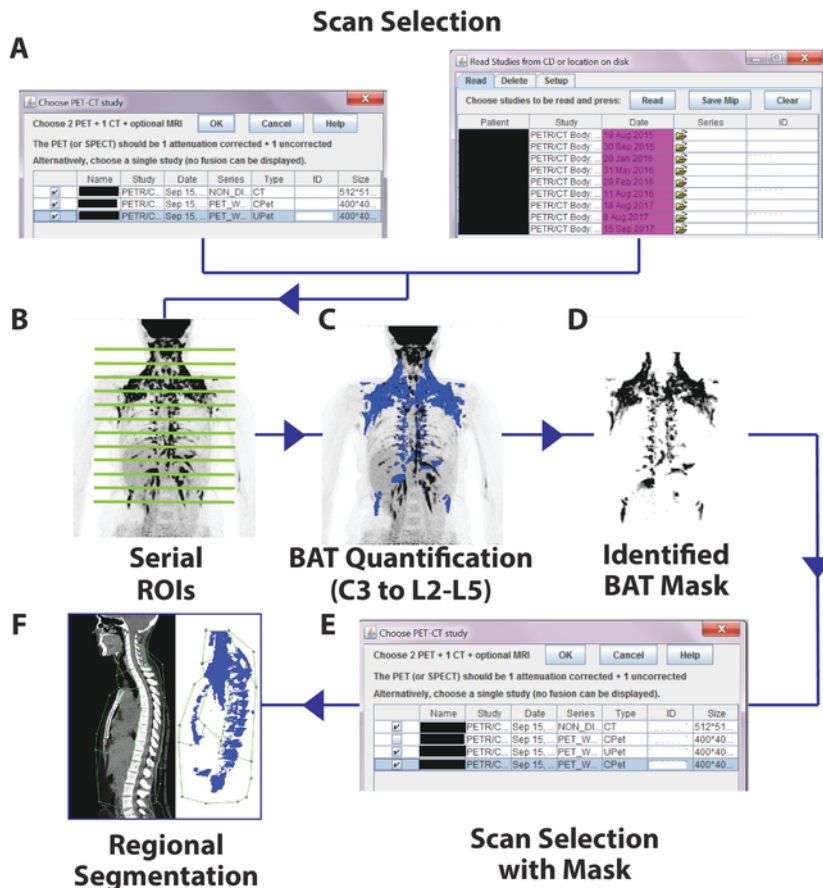


**Figure 1. Schematic Flow of the Image Processing Steps.** First, PET images and corresponding CT images are uploaded into the PET/CT plug-in (A). After axial ROIs are drawn on each PET/CT slice (B), each voxel meeting both PET and CT criteria are identified in blue (C). A mask is generated from these BAT-identified voxels (D), which is substituted for the original corrected PET scan (E), and depots are segmented in the sagittal view (F). [Please click here to view a larger version of this figure.](#)

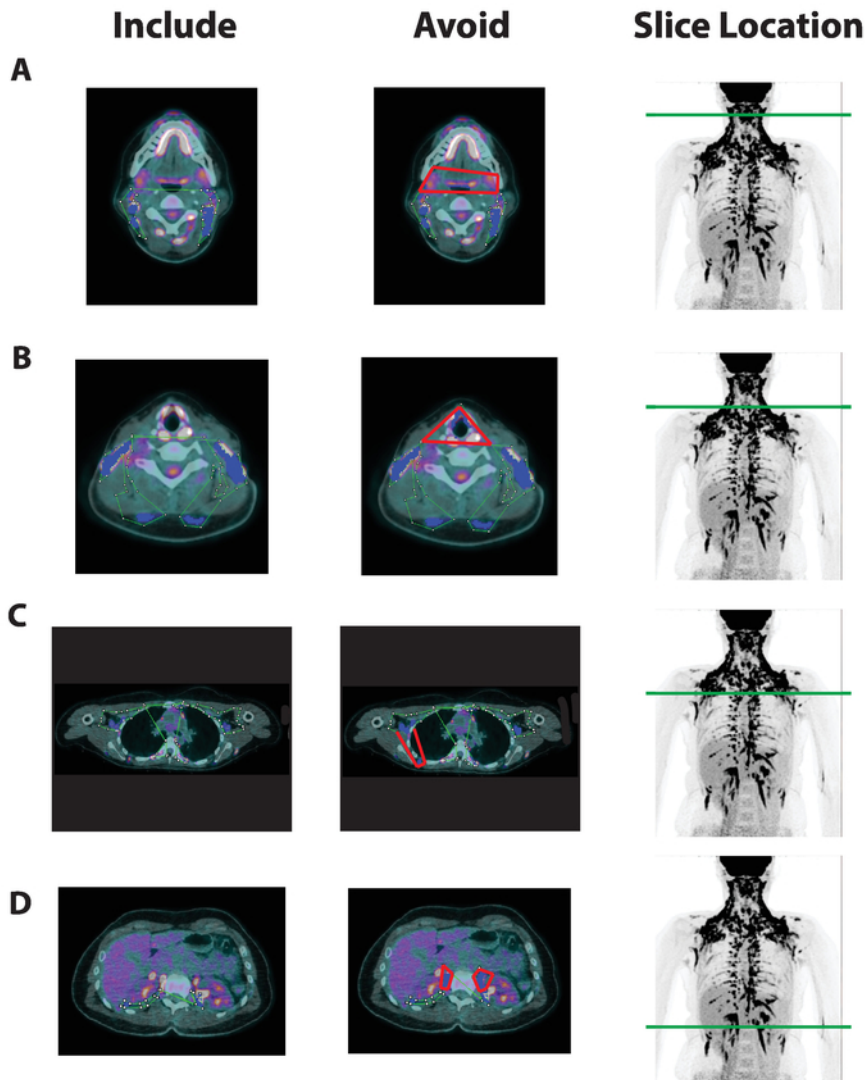


**Figure 2. Axial BAT Region-of-Interest Selection and Common Areas To Avoid in Multiple BAT Depots.** Axial slices from a fused PET/CT image (columns 1 and 2) and a maximal intensity projection image (MIP, column 3) with green lines to denote slice height from a scan acquired following cold-stimulation. Green ROIs are drawn around areas with adipose tissue density, high FDG uptake, and anatomical locations likely to contain active BAT in columns 1 and 2. Anatomical areas unlikely to contain BAT are highlighted in red in column 2. Voxels meeting the BAT PET and CT criteria are confirmed by ImageJ and highlighted in blue. Examples are taken from the (A) anterior cervical depot, (B) cervical depot at the level of the thyroid, (C) Supraclavicular/Axillary depot nearby shivering skeletal muscle (*i.e.*, Intercostals), and (D) the Abdominal depot at the level of the ureters of the kidneys. [Please click here to view a larger version of this figure.](#)

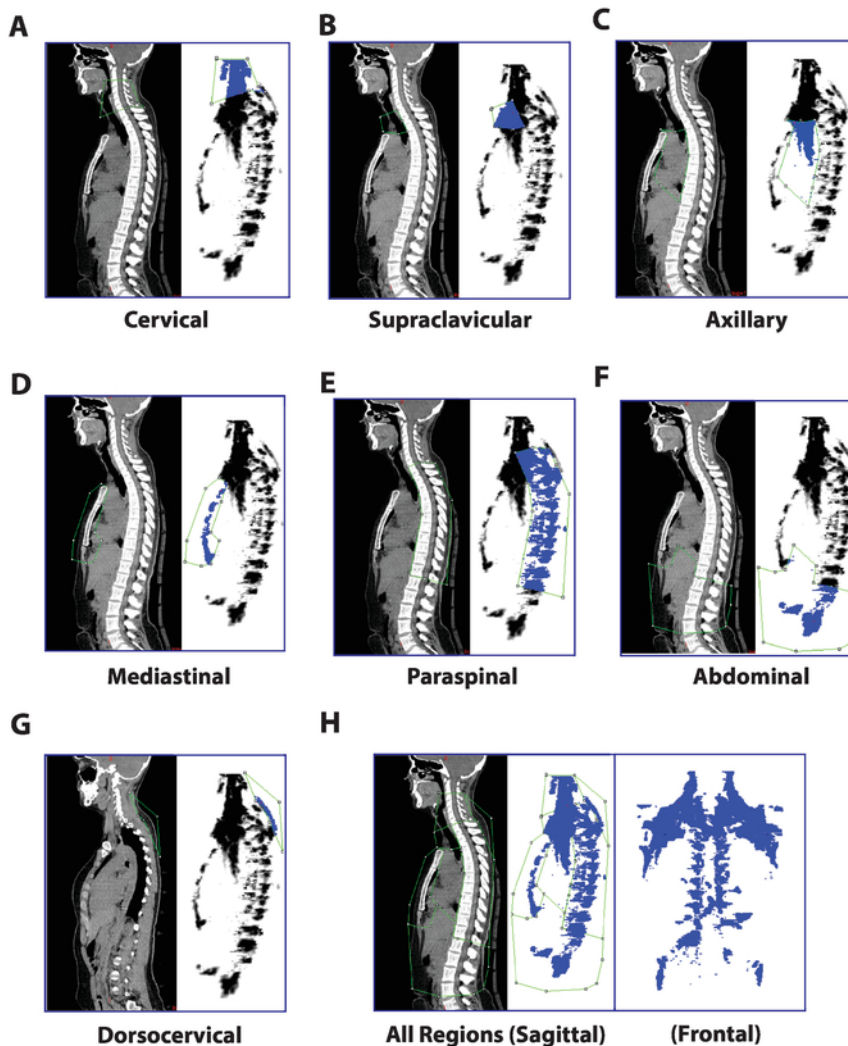


**Figure 3. Regional Segmentation of Seven BAT Depots in the Sagittal View.** Following the generation of a "BAT mask" image containing only PET voxels previously identified as active BAT, the following regions can be separated with ROIs drawn in the sagittal plane: (A) Cervical (C3-C7), (B) Supraclavicular (C7-T3, excluding vertebrae), (C) Axillary (T3-T7, excluding vertebrae), (D) Mediastinal (anterior mediastinum), (E) Paraspinal (T1-T12, from the anterior edge of the vertebrae to the spinous processes), (F) Abdominal (T12-L3, retroperitoneal), and (G) Dorsocervical (fat depot distinct and posterior to the paraspinal depot; near the cervical region). The composite image with all regions appears in (H). [Please click here to view a larger version of this figure.](#)

## Discussion

Since confirmation of functional BAT in adult humans, there has been great interest in understanding the role of BAT in human physiology. However, because this thermogenic tissue is often found in narrow fascial planes, interspersed within white fat, and surrounding other organs, it is challenging to quantify. In 2016, a consensus document was published by an International BAT expert panel with recommendations for reporting relevant participant characteristics, criteria for subject preparation, and a protocol for acquiring PET/CT images<sup>21</sup>. The panel also identified the need for more consistency in the processing of PET/CT for BAT quantification, noting that methods to identify BAT have varied widely and, in most cases, only limited detail of the BAT quantification procedure is provided. Consequently, while reports of within study reproducibility are high<sup>22,23,24</sup>, appreciably different BAT volume and activity has been reported by groups using different quantification methods, even when participants are of similar age, sex, and BMI<sup>25,26</sup>. These inconsistencies make comparing findings difficult, and have led to a controversy over the amount of BAT in the adult human<sup>15</sup>.

An inherent limitation of PET/CT image processing is the inclusion of voxels that meet both PET and CT criteria but are in anatomical locations that correspond to structures other than BAT. Perfect co-registration of PET and CT images is nearly impossible due to differences in resolution and subject motion during scans. As a consequence, structures bordering air or bone and regions of high tracer uptake are often incorrectly identified as active BAT. To limit inclusion of false positive voxels, one should apply PET and CT criteria only within the ROIs that users construct. But current approaches to quantify BAT with user-specified ROIs or automated analyses differ in the amount of user involvement and knowledge they require. We have shown that using a single, two-dimensional user-defined coronal ROI applied to the entire stack of images may be more prone to including false positive areas<sup>19</sup>. Several groups have developed automated methods to quantify BAT that are capable of rapidly processing large datasets without much user input. However, these methods either fail to include all potential BAT-containing regions, particularly

in the lower body<sup>27</sup>, or incur relatively high rates of false positives<sup>28</sup> and false negatives<sup>26</sup>. Since the volume of human BAT is generally low (<600 mL, or <2% of total body mass), small absolute errors in quantification may lead to large relative differences.

The more rigorous approach described by this study of drawing ROIs on each axial PET-CT slice allows the detection of BAT in narrow fascial layers while providing more confidence that false positives have been excluded. This yields a detailed quantification in each individual, rather than a binary assessment of BAT's presence or absence<sup>29</sup>. Therefore, it may be more suitable for controlled experiments in small sample sizes intending to study BAT physiology and/or effects from interventions. Furthermore, the ability to define region-specific BAT depots may provide more insight into BAT's functional relevance and developmental origin. We believe these quantitative measures are important not only for comparison across the field, but also to better estimate BAT's contribution to energy metabolism and thermoregulation in adult humans.

Several anatomical features of BAT will help users of our method limit inclusion of false positive voxels. BAT is typically found in continuous and symmetric fascial layers. Thus, while drawing and refining an ROI, examining the superior and inferior axial slices for continuity and symmetry of the selected adipose tissue can help users maximize inclusion of adipose tissue while minimizing inclusion of skeletal muscle, bone, and other obvious non-BAT structures. Active BAT is also rarely present in subcutaneous adipose depots, so we advise users to avoid these areas when constructing ROIs. As noted in the protocol, BAT is distributed in several distinct anatomical regions, including the cervical, dorsocervical, supraclavicular, axillary, mediastinal, paraspinous, and abdominal depots. These depots are distributed such that one axial slice may contain more than BAT from multiple depots. For instance, an axial slice in the thoracic region can contain BAT from the mediastinal depot (proximal and anterior), paraspinous depot (proximal and posterior, along the spine), and axillary depot (lateral and near the mid-antero-posterior line). Knowledge of these depots can help users create ROIs in the various regions of the body, since they occur in pre-described locations are largely contiguous, as described in our protocol. However, because we encourage users to draw only one ROI per slice to avoid ROI overlap, the additional steps of generating a BAT mask and drawing sagittal ROIs is required to separate the previously-identified BAT voxels into the distinct regional depots if information of BAT distribution is desired, *i.e.*, separating mediastinal, paraspinous, and axillary BAT detected in the same axial ROI into depots based on sagittal location (**Figure 3**).

The PET/CT viewer software can also be used to quantify the activity of tissues other than BAT, for instance shivering skeletal muscle, which also major plays a role cold induced thermogenesis<sup>19</sup>, or various areas of the brain or liver that have been suggested as reference tissues for PET/CT analysis<sup>21</sup>. However, these tissues will have densities and anatomical distributions that differ from BAT and are outside the focus of our current protocol. We direct readers to the consensus document for greater detail on these subjects<sup>21</sup>. Finally, we advise all users to continually update ImageJ and visit [petctviewer.org](http://petctviewer.org) for Plug-in updates and software assistance.

Though we believe that this rigorous method is more precise than automated methods<sup>26,28</sup> and methods that use a simplified, single ROI to estimate total BAT volume<sup>9,30</sup>, it is not without limitations. There is no ideal method to non-invasively quantify BAT in humans, and <sup>18</sup>F-FDG represents only glucose uptake, which is not the same as glucose metabolism<sup>11</sup>. However, even though other radioactive tracers have been used<sup>31,32,33</sup>, <sup>18</sup>F-FDG is the most prominent tracer used to study human BAT. Thus, developing standardized methods to analyze <sup>18</sup>F-FDG PET/CT images will continue to be impactful in the study of human BAT physiology for the foreseeable future.

The method we propose, creating an ROI on each BAT-containing axial slice while avoiding common problem areas, is labor intensive and requires the user to have some knowledge of underlying anatomy. It is also possible that the stringent ROI selection may introduce false negatives, since some BAT-containing depots may be avoided. Drawing ROIs on every axial slice of the fused PET/CT image allows for careful discrimination between adipose tissue and neighboring metabolically active tissues and/or regions impacted by spill over and partial volume effects<sup>34</sup>. However, the time it takes to complete analysis of a single scan can range from three to eight hours, with the possibility of shortening the time frame with practice and experience. Various machine learning approaches may be able to reduce the labor and expertise required to accomplish this task. However, creating a more automated method that can accurately detect BAT and is robust to false positives created by current imaging limitations will require a large dataset with individuals of varied body composition and BAT distribution. We hope that this method can be used to produce a detailed BAT atlas that may serve as a template for more sophisticated big data approaches.

In conclusion, we demonstrated a step-by-step image analysis approach to quantify human brown adipose tissue volume, activity, and distribution using cold-induced FDG PET/CT scans. The critical steps include 1) continuously and sequentially analyzing axial ROIs and 2) assessing relevant BAT depots by their anatomical location while avoiding other metabolically active tissues. This rigorous quantification approach can be used by investigators in the field to study BAT physiology and serve as reference standard for developing automated human BAT quantitation approaches in the future.

## Disclosures

The authors have nothing to disclose.

## Acknowledgments

We would like to thank all of the study volunteers, nursing and clinical staff, and the dieticians of the NIH Clinical Center for their participation in our cold exposure studies and care provided during the inpatient stays. We'd also like to thank Dr. Bill Dieckmann for all of his assistance with the acquisition and distribution of the PET-CT images for our studies. This work was supported by Intramural Research Program of the National Institute of Diabetes and Digestive and Kidney Diseases Grants Z01 DK071014 (to K.Y.C.) and DK075116-02 (to A.M.C.).

## References

1. Bovet, P., Chioloro, A., Gedeon, J. Health effects of overweight and obesity in 195 countries. *The New England Journal of Medicine*. **377** (15), 1495-1496 (2017).
2. Maughan, R. Carbohydrate metabolism. *Surgery (Oxford)*. **27** (1), 6-10 (2009).

3. Cypess, A.M. *et al.* Identification and importance of brown adipose tissue in adult humans. *The New England Journal of Medicine*. **360** (15), 1509-1517 (2009).
4. van Marken Lichtenbelt, W.D. *et al.* Cold-activated brown adipose tissue in healthy men. *The New England Journal of Medicine*. **360** (15), 1500-1508 (2009).
5. Virtanen, K.A. *et al.* Functional brown adipose tissue in healthy adults. *The New England Journal of Medicine*. **360** (15), 1518-1525 (2009).
6. Abreu-Vieira, G., Xiao, C., Gavrilova, O., Reitman, M.L. Integration of body temperature into the analysis of energy expenditure in the mouse. *Molecular Metabolism*. **4** (6), 461-470 (2015).
7. Cypess, A.M., Kahn, C.R. Brown fat as a therapy for obesity and diabetes. *Current Opinion in Endocrinology, Diabetes, and Obesity*. **17** (2), 143-149 (2010).
8. Orava, J. *et al.* Different metabolic responses of human brown adipose tissue to activation by cold and insulin. *Cell Metabolism*. **14** (2), 272-279 (2011).
9. Chen, K.Y. *et al.* Brown fat activation mediates cold-induced thermogenesis in adult humans in response to a mild decrease in ambient temperature. *The Journal of Clinical Endocrinology and Metabolism*. **98** (7), E1218-1223 (2013).
10. Ouellet, V. *et al.* Brown adipose tissue oxidative metabolism contributes to energy expenditure during acute cold exposure in humans. *The Journal of Clinical Investigation*. **122** (2), 545-552 (2012).
11. Blondin, D.P. *et al.* Contributions of white and brown adipose tissues and skeletal muscles to acute cold-induced metabolic responses in healthy men. *The Journal of Physiology*. **593** (3), 701-714 (2015).
12. Ruiz, J.R., Martinez-Tellez, B., Sanchez-Delgado, G., Aguilera, C.M., Gil, A. Regulation of energy balance by brown adipose tissue: at least three potential roles for physical activity. *British Journal of Sports Medicine*. **49** (15), 972-973 (2015).
13. Bakker, L.E.H. *et al.* Brown adipose tissue volume in healthy lean south Asian adults compared with white Caucasians: a prospective, case-controlled observational study. *The Lancet Diabetes & Endocrinology*. **2** (3), 210-217 (2014).
14. Lee, P. *et al.* Temperature-acclimated brown adipose tissue modulates insulin sensitivity in humans. *Diabetes*. **63** (11), 3686-3698 (2014).
15. Jensen, M.D. Brown adipose tissue - not as hot as we thought. *The Journal of Physiology*. **593** (3), 489-490 (2015).
16. Heaton, J.M. The distribution of brown adipose tissue in the human. *Journal of Anatomy*. **112** (Pt 1), 35-39 (1972).
17. Chauvie, S., Bertone, E., Bergesio, F., Terulla, A., Botto, D., Cerello, P. Automatic liver detection and standardised uptake value evaluation in whole-body Positron Emission Tomography/Computed Tomography scans. *Computer Methods and Programs in Biomedicine*. **156**, 47-52 (2018).
18. Chondronikola, M., Beeman, S.C., Wahl, R.L. Non-invasive methods for the assessment of brown adipose tissue in humans. *The Journal of Physiology*. **596** (3), 363-378 (2018).
19. Leitner, B.P. *et al.* Mapping of human brown adipose tissue in lean and obese young men. *Proceedings of the National Academy of Sciences of the United States of America*. **114** (32), 8649-8654 (2017).
20. Martinez-Tellez, B. *et al.* The impact of using BARCIST 1.0 criteria on quantification of BAT volume and activity in three independent cohorts of adults. *Scientific Reports*. **8** (1), 8567 (2018).
21. Chen, K.Y. *et al.* Brown Adipose Reporting Criteria in Imaging STudies (BARCIST 1.0): recommendations for standardized FDG-PET/CT experiments in humans. *Cell Metabolism*. **24** (2), 210-222 (2016).
22. Rasmussen, J.M. *et al.* Brown adipose tissue quantification in human neonates using water-fat separated MRI. *PloS One*. **8** (10), e77907 (2013).
23. Becker, A.S. *et al.* In-depth analysis of interreader agreement and accuracy in categorical assessment of brown adipose tissue in (18)FDG-PET/CT. *European Journal of Radiology*. **91**, 41-46 (2017).
24. Lee, Y.-H., Hsiao, H.-F., Yang, H.-T., Huang, S.-Y., Chan, W.P. Reproducibility and repeatability of computer tomography-based measurement of abdominal subcutaneous and visceral adipose tissues. *Scientific Reports*. **7**, 40389 (2017).
25. Lundström, E., Strand, R., Johansson, L., Bergsten, P., Ahlström, H., Kullberg, J. Magnetic resonance imaging cooling-reheating protocol indicates decreased fat fraction via lipid consumption in suspected brown adipose tissue. *PLOS One*. **10** (4), e0126705 (2015).
26. Gifford, A., Towse, T.F., Walker, R.C., Avison, M.J., Welch, E.B. Human brown adipose tissue depots automatically segmented by positron emission tomography/computed tomography and registered magnetic resonance images. *Journal of Visualized Experiments*. (96) (2015).
27. Jones, T.A. *et al.* Brown fat depots in adult humans remain static in their locations on PET/CT despite changes in seasonality. *Physiological Reports*. **5** (11) (2017).
28. Ruth, M.R., Wellman, T., Mercier, G., Szabo, T., Apovian, C.M. An automated algorithm to identify and quantify brown adipose tissue in human 18F-FDG-PET/CT scans. *Obesity (Silver Spring, Md.)*. **21** (8), 1554-1560 (2013).
29. Hibi, M. *et al.* Brown adipose tissue is involved in diet-induced thermogenesis and whole-body fat utilization in healthy humans. *International Journal of Obesity (2005)*. **40** (11), 1655-1661 (2016).
30. Hanssen, M.J.W. *et al.* Short-term cold acclimation recruits brown adipose tissue in obese humans. *Diabetes*. **65** (5), 1179-1189 (2016).
31. Muzik, O., Mangner, T.J., Leonard, W.R., Kumar, A., Janisse, J., Granneman, J.G. 15O PET measurement of blood flow and oxygen consumption in cold-activated human brown fat. *Journal of Nuclear Medicine: Official Publication, Society of Nuclear Medicine*. **54** (4), 523-531 (2013).
32. Blondin, D.P. *et al.* Inhibition of intracellular triglyceride lipolysis suppresses cold-induced brown adipose tissue metabolism and increases shivering in humans. *Cell Metabolism*. **25** (2), 438-447 (2017).
33. Admiraal, W.M., Holleman, F., Bahler, L., Soeters, M.R., Hoekstra, J.B., Verberne, H.J. Combining 123I-metaiodobenzylguanidine SPECT/CT and 18F-FDG PET/CT for the assessment of brown adipose tissue activity in humans during cold exposure. *Journal of Nuclear Medicine: Official Publication, Society of Nuclear Medicine*. **54** (2), 208-212 (2013).
34. Soret, M., Bacharach, S.L., Buvat, I. Partial-volume effect in PET tumor imaging. *Journal of Nuclear Medicine: Official Publication, Society of Nuclear Medicine*. **48** (6), 932-945 (2007).